ELSEVIER

Microporous and Mesoporous Materials 27 (1999) 261–271

MICROPOROUS AND MESOPOROUS MATERIALS

Characterization of the acid sites in MCM-41-type materials by spectroscopic and catalytic techniques

M. Hunger, U. Schenk, M. Breuninger, R. Gläser, J. Weitkamp *

Institute of Chemical Technology I, University of Stuttgart, D-70550 Stuttgart, Germany

Received 7 November 1997; received in revised form 27 January 1998; accepted 27 January 1998

Abstract

Temperature-programmed desorption of pyridine, FTIR and multinuclear NMR spectroscopy and catalytic test reaction have been applied to investigate acid sites in mesoporous materials with silicon/aluminum ratios of 266 and 20 and in an amorphous aluminosilicate with $n_{Si}/n_{Al} = 5.4$. The results obtained by these methods indicate the presence of weak Brønsted acid sites in the aluminosilicate samples. Based on the spectroscopic data, a model of Brønsted acid sites in the aluminum-containing MCM-41 is proposed which consists of silanol groups with 3–4 framework aluminum atoms in their local structure. In the dehydrated ammonium form of the mesoporous aluminosilicate, these framework aluminum atoms have a tetrahedral oxygen coordination. Deammoniation leads to a strong broadening of the ^{27}Al echo NMR signal due to framework aluminum atoms which indicates a variation of their local geometry and/or oxygen coordination. ^{27}Al echo NMR studies of calcined and subsequently reammoniated samples indicate that this variation in the bonding state of framework aluminum atoms is a reversible process. © 1999 Elsevier Science B.V. All rights reserved.

Keywords: Brønsted acid sites; Catalytic test reactions; FTIR spectroscopy; MCM-41; Solid-state NMR spectroscopy

1. Introduction

MCM-41, a member of the M41S family, possesses a hexagonal arrangement of uniformly sized mesopores with diameters in the range 1.5–10 nm. With the advent of these materials, the pore size range of inorganic molecular sieves has been dramatically expanded. Since the re-discovery of MCM-41 by scientists of Mobil Oil Corporation in 1992 [1] (it appears that practically the same material has been described as early as 1969 [2]) a number of publications were dealing with the synthesis of MCM-41 [3–5], its sorptive properties [6–8], its application as a host material for various guest compounds [9–11], and the behavior of isomorphously substituted mesoporous materials [12–14]. For the application of MCM-41 in catalysis, a detailed knowledge is desirable concerning the acid sites existing in the mesopores of the aluminum-containing material. Even though these sites were investigated earlier by different spectroscopic techniques [15–21], many questions remained open and their chemical nature is largely unknown. FTIR spectra of calcined MCM-41 consist of bands at 3745 cm^{-1} due to isolated silanol groups and at 3715 and 3530 cm^{-1} caused

* Corresponding author. Tel: +49 711 685 4060; Fax: +49 711 685 4065; E-mail: jens.weitkamp@po.uni-stuttgart.de

1387-1811/99/$ – see front matter © 1999 Elsevier Science B.V. All rights reserved.
PII: S1387-1811(98)00260-1

by hydrogen-bound internal SiOH groups [19]. Upon increasing the aluminum content (from $n_{Si}/n_{Al}=100$ to 13), Jentys et al. [19] found an additional broad band at ca. 3660 cm^{-1} which they assigned to hydroxyl groups on octahedrally coordinated aluminum species. After adsorption of deuterated acetonitrile on calcined MCM-41 ($n_{Si}/n_{Al}=40$), Busio et al. [16] observed bands in the C–N frequency region at 2275 and 2331 cm^{-1} which the authors attributed to CD_3CN adsorbed on terminal SiOH groups and on aluminum atoms bound to three silicon atoms, respectively. The threefold coordinated aluminum atoms were proposed to be created by dehydration of Brønsted acid sites [16]. Liepold et al. [18] explained the catalytic activity of calcined MCM-41 ($n_{Si}/n_{Al}=17.3$) in cracking of *n*-hexadecane by weak Brønsted acid sites interacting with neighboring coordinatively unsaturated aluminum species which synergistically form Brønsted acid sites.

In the present work, temperature-programmed desorption (TPD) of pyridine, FTIR and multinuclear NMR spectroscopy and catalytic test reaction were applied to characterize the acid sites in siliceous and aluminum-containing mesoporous materials and an amorphous aluminosilicate.

2. Experimental section

The amorphous aluminosilicate (sample AAS/5.4) with a silicon to aluminum ratio of 5.4 is a commercial product which has kindly been supplied by Akzo Corporate Research, Obernburg, Germany. Mesoporous MCM-41 materials with n_{Si}/n_{Al} ratios of 266 (sample MCM-41/266) and 20 (sample MCM-41/20) were synthesized as described elsewhere [8]. To eliminate the organic template molecules, the as-synthesized materials were heated with a rate of 1 K min^{-1} from room temperature to a final temperature of 773 K in a flow (1000 cm^3 min^{-1}) of dry nitrogen at 100 kPa. After 300 min at this temperature, 10 vol.% oxygen was added to the flow (30 cm^3 min^{-1}) of nitrogen. The acidic forms of all samples were prepared by a treatment of the powdered materials with a 1 M aqueous solution of NH_4NO_3 at 353 K and subsequent calcination at 673 K for 12 h in dry nitrogen at 100 kPa (flow rate 1000 cm^3 min^{-1}).

The compositions of the calcined samples were determined by atomic absorption spectrometry after dissolution in diluted hydrofluoric acid (10 wt.% HF). The X-ray powder patterns were recorded over the 2θ range 1.5–7° using a Siemens D5000 instrument in the step-scan mode (step width of 0.01°) using CuKα-radiation. The adsorption isotherms for nitrogen (BET) were measured at 77 K on a Micromeritics ASAP 2010 instrument. Prior to these measurements, the samples were degassed ($p<10^{-1}$ Pa) at 523 K for 2 h.

Both the catalytic tests and the temperature-programmed desorption (TPD) of pyridine were performed at atmospheric pressure using a flow-type fixed bed reactor/adsorber and *on-line* gas-chromatographic analysis of the reactor/adsorber effluent with a flame ionization detector. Ethylbenzene (E-Bz) and methanol (Me), both analytical grade, were purchased from Merck, Darmstadt. MCM-41 powder was pressed binder-free, crushed and sieved into particles with diameters between 0.2 and 0.3 mm. Prior to the catalytic investigations, the samples were heated with a rate of 3 K min^{-1} to the final temperature of 523 K (disproportionation of E-Bz) or 723 K (conversion of Me) and purged at the same temperature with dry nitrogen (50 cm^3 min^{-1}) for 12 h. The ethylbenzene disproportionation was carried out at a reaction temperature of 523 K, an E-Bz partial pressure of 1 kPa and a modified residence time of $W/F_{E\text{-}Bz}=1870$ g h mol^{-1}. For the conversion of methanol, a reaction temperature of 723 K, a methanol partial pressure of 15 kPa and a modified residence time of $W/F_{Me}=300$ g h mol^{-1} were applied.

Prior to the TPD experiments, the crushed and sieved materials were calcined at 523 K in dry nitrogen (30 cm^3 min^{-1}) for 6 h and loaded with pyridine (Py, analytical grade, purchased from Merck, Darmstadt) at 453 K in a flow of nitrogen (40 cm^3 min^{-1}) with a Py partial pressure of 13 mbar. Subsequently, the samples were purged at the same temperature with dry nitrogen (30 cm^3 min^{-1}) until no pyridine was detected any more in the adsorber effluent. The temperature-programmed desorption of pyridine was performed

in the temperature range 473–1073 K with a nitrogen flow of 30 $cm^3\,min^{-1}$, a heating rate of 5 K min^{-1} and sampling of the desorbed molecules in intervals of 2 min.

The FTIR spectra were recorded using a Perkin-Elmer 1760X spectrometer with a resolution of 4 cm^{-1}. Thin self-supporting wafers (3–7 mg cm^{-2}) were prepared and placed in an in-situ cell which allowed for calcination of the wafers in vacuo and recording of the FTIR spectra during adsorption and desorption of probe molecules. After calcination of the samples in vacuo ($p<10^{-4}$ Pa) at 673 K for 12 h, pyridine was adsorbed at 393 K with a partial pressure of 3.4 mbar. Weakly physisorbed pyridine molecules were removed by desorption at 453 K for at least 2 h, until a pressure of 10^{-4} Pa or less was reached.

The NMR experiments were carried out on a Bruker MSL 400 spectrometer at resonance frequencies of 79.5 MHz for ^{29}Si, 104.3 MHz for ^{27}Al and 400.1 MHz for ^{1}H nuclei. For the ^{29}Si MAS NMR investigations a 7 mm double-bearing Bruker MAS probe with a sample spinning rate of 3.5 kHz was used, while all other experiments were carried out applying a 4 mm double-bearing Bruker MAS probe at a spinning rate of 10 kHz. The ^{27}Al echo NMR spectra were recorded on static samples (without MAS) as described in Ref. [22] with a phase-cycled quadrupole-echo sequence and using a pulse and echo delay of 10 μs. Prior to the ^{27}Al echo and ^{1}H MAS NMR studies the powder material was calcined at 673 K for 12 h in vacuo ($p<10^{-3}$ Pa). Perdeuterated pyridine (C_5ND_5, 99 atom%, lot no. UN 1282, Aldrich Chemical Company, Inc.) was adsorbed onto the calcined samples at a partial pressure of 10 mbar using a vacuum line. After adsorption, the weakly physisorbed probe molecules were removed by desorption at room temperature for 2 h, until a pressure of 10^{-3} Pa or lower was reached. Finally, the samples were sealed in symmetric glass ampoules with an outer diameter of 3.0 mm allowing a sample spinning with rates of up to 12 kHz.

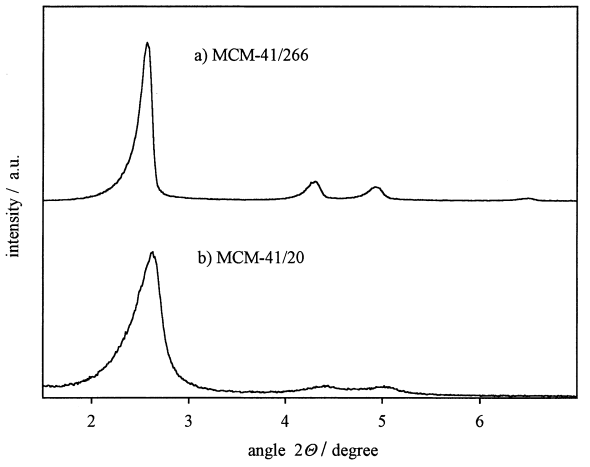


Fig. 1. XRD patterns of the calcined (673 K) mesoporous materials: (a) MCM-41/266; and (b) MCM-41/20.

3. Results and discussion

3.1. X-ray diffraction

The XRD patterns (Fig. 1) of the calcined (673 K) and rehydrated mesoporous materials MCM-41/266 and MCM-41/20 consist of the typical strong reflexion at 2.5° and weak reflexions at 4.1, 4.8 and 6.5° which correspond to *d* spacings of ca. 36, 25, 22 and 17 Å, respectively. In agreement with the literature [3,15,17], the aluminosilicate MCM-41/20 [Fig. 1(b)] gives a lower quality pattern than the siliceous MCM-41/266 [Fig. 1(a)]. This indicates that, due to the incorporation of aluminum atoms, the local structure of the aluminosilicate MCM-41/20 is less uniform than that of the purely siliceous material [17].

3.2. ^{29}Si and ^{27}Al MAS NMR spectroscopy of the rehydrated mesoporous materials

Fig. 2 shows the ^{29}Si MAS NMR spectra (left) of the calcined (673 K) and rehydrated samples MCM-41/266 (a); MCM-41/20 (b); and AAS/5.4 (c). All spectra consist of broad signals at ca. −90, −100 and −110 ppm. According to Kolodziejski et al. [5], the strongest signal at ca. −110 ppm is due to $Si(OSi)_4$ sites, while the shoulders at −90 and −100 ppm are due to $Si(OSi)_2(OH)_2$ and $Si(OSi)_3OH$ sites, respectively. Considering the different aluminum contents of the samples under study (Table 1, column 2), a contribution of

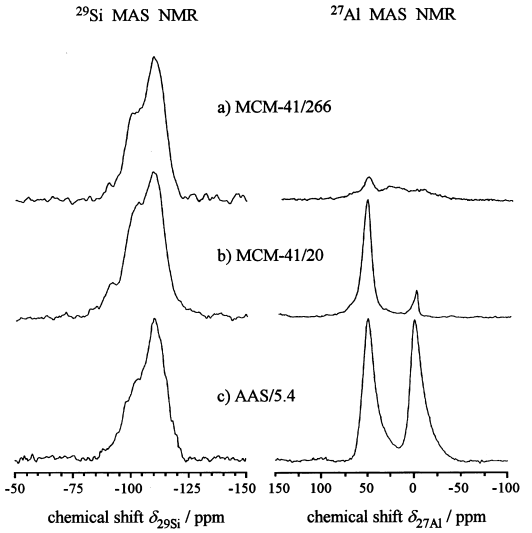


Fig. 2. ^{29}Si MAS NMR (left) and ^{27}Al MAS NMR (right) spectra of the mesoporous materials: (a) MCM-41/266; (b) MCM-41/20; and (c) the amorphous aluminosilicate AAS/5.4 recorded after calcination at 673 K and rehydration.

$Si(OSi)_3(OAl)$, $Si(OSi)_2(OAl)_2$ and $Si(OSi)(OAl)_3$ sites to the signals at -100 and -90 ppm has to be expected. These signals may be the reason for the stronger low-field shoulders in the ^{29}Si MAS NMR spectrum of MCM-41/20 [Fig. 2(b), left].

The ^{27}Al MAS NMR spectra (Fig. 2, right) of the calcined (673 K) and rehydrated materials show signals at 52–54 ppm due to tetrahedrally coordinated framework aluminum and at 0–30 ppm caused by distorted or octahedrally coordinated aluminum atoms at extra-framework positions or in a separate phase [3]. The low intensities of the ^{27}Al MAS NMR signals of MCM-41/266 agree with the low aluminum content of this sample (Table 1, column 2). The high intensity of the contribution at 0–30 ppm indicates that most of these aluminum atoms are not incorporated into the framework. While the ^{27}Al MAS NMR spectrum of the as-synthesized MCM-41/20 (not shown) consists of a single signal at 52 ppm, the signal at 0 ppm appearing in Fig. 2(b) (right) indicates a partial dealumination of this sample as a result of calcination at 673 K. However, most of the aluminum atoms remain in a tetrahedral oxygen coordination at framework positions. In contrast to Busio et al. [16], no high-field shift of the resonance position of the tetrahedrally coordinated framework aluminum was found.

A significantly different situation is encountered for the amorphous aluminosilicate AAS/5.4. The ^{27}Al MAS NMR spectrum of this sample (Fig. 2c, right) shows two signals at 54 and 4 ppm with nearly equal intensities, caused by tetrahedrally and octahedrally coordinated aluminum atoms, respectively. Interestingly, a similar observation

Table 1
Aluminum contents; surface areas, A_{BET}; conversions of ethylbenzene, $X_{E\text{-}Bz}$; yields of hydrocarbons in the C_1–C_5 range, Y_{HC}, obtained in the conversion of methanol; amount of strongly adsorbed pyridine; and concentrations of hydroxyl groups, c_{OH}; and ammonium ions, c_{NH4}

Sample	Aluminum content (mmol g^{-1})	A^a_{BET} (m^2 g^{-1})	Conversion of E-Bz[b] $X_{E\text{-}Bz}$ (%)	Yield of hydrocarbons[c] Y_{HC} (%)	Desorbed pyridine[d] (mmol g^{-1})	c^e_{OH} (mmol g^{-1})	c^f_{NH4} (mmol g^{-1})
MCM-41/266	0.062	850	0.3	2.2	0.030	2.70	*
MCM-41/20	0.794	860	1.2	14.1	0.365	2.56	0.18
AAS/5.4	2.600	460	2.5	7.6	0.183	1.20	0.06

[a] Surface area determined by adsorption of nitrogen (BET).
[b] Ethylbenzene (E-Bz) disproportionation, $T_R = 523$ K, $W/F_{E\text{-}Bz} = 1870$ g h mol^{-1}, time on stream = 6 h.
[c] Conversion of methanol, $T_R = 723$ K, $W/F_{Me} = 300$ g h mol^{-1}, time on stream = 10 h.
[d] Temperature-programmed desorption (TPD) of pyridine (see Fig. 3).
[e] Concentration of hydroxyl groups of the calcined (673 K) samples determined by ^{1}H MAS NMR spectroscopy (accuracy: $\pm$10%).
[f] Concentration of strongly bound ammonium ions determined by ^{1}H MAS NMR spectroscopy after dehydration at 473 K (accuracy: $\pm$10%).
* Deconvolution of the ^{1}H MAS NMR spectrum not possible.

has been made by Busio et al. [16] when studying MCM-41 with a silicon to aluminum ratio of 5.

3.3. Catalytic investigations

The disproportionation of ethylbenzene has been demonstrated earlier to be a suitable catalytic test reaction for probing the Brønsted acidity of large pore zeolites [23–25]. At reaction temperatures of 433–493 K, where acidic forms, e.g. of zeolite Y, typically show ethylbenzene conversions of 10%–15% [25], no conversion at all was observed over the samples MCM-41/266, MCM-41/20 and AAS/5.4. Therefore, the reaction temperature had to be raised to 523 K which is the upper temperature limit beyond which undesirable side reactions usually begin to occur. At this reaction temperature the steady state was reached after a time-on-stream of 6 h leading to the ethylbenzene conversions summarized in column 4 of Table 1. While over MCM-41/20 nearly equal amounts (ca. 45%) of the isomers 1,3-diethylbenzene and 1,4-diethylbenzene were found, over AAS/5.4 the isomer 1,3-diethylbenzene was preferentially formed (58%). Since the latter is characteristic for acidic zeolites, the observed isomer distributions are in line with the conversions of ethylbenzene found for MCM-41/20 ($X_{\text{E-Bz}} = 1.2\%$) and AAS/5.4 ($X_{\text{E-Bz}} = 2.5\%$).

The conversion of methanol over strongly acidic catalysts, such as H-ZSM-5, in the MTG-process (methanol to gasoline) at reaction temperatures of 613–753 K yields hydrocarbons as the main products [26,27]. Using catalysts of weak acidity, conversion of methanol results in the formation of dimethylether, which is an intermediate in the methanol to hydrocarbons reaction over strongly acidic catalysts [26,27]. In the present study a reaction temperature of 723 K was chosen leading to methanol conversions of 51–68% for all samples under study. Interestingly, the yield of dimethylether (10.3%) was highest for the siliceous MCM-41/266. We conclude that silanol groups occurring in large concentrations in MCM-41/266 (vide infra) could be responsible for the conversion of methanol to dimethylether (DME) at 723 K. The absence of strong Brønsted acid sites prevents the consecutive conversion of this intermediate into hydrocarbons. Another situation is encountered with the aluminosilicates MCM-41/20 and AAS/5.4. These samples show a much higher yield of hydrocarbons in the C_1–C_5 range (Table 1, column 5) indicating the presence of Brønsted acid sites which are strong enough to catalyze the consecutive conversion of DME under the reaction conditions applied here.

3.4. Temperature-programmed desorption of pyridine

In Fig. 3 the temperature-programmed desorption spectra of pyridine on the mesoporous materials MCM-41/266 and MCM-41/20 and the amorphous aluminosilicate AAS/5.4 are depicted. The amount of desorbed pyridine which corresponds to the integral intensity of the desorption curves recorded in the temperature range 473–1073 K is given in column 6 of Table 1. According to these values, the mesoporous material MCM-41/20 has the largest number of strong adsorption sites for pyridine. As shown in Fig. 3, the desorption curve of this sample consists of a low-temperature peak with a maximum at 580 K and a high-temperature peak with a maximum at 910 K. In previous work on TPD of pyridine from zeolites HY [28], the desorption peaks at 665–690 K and 770–810 K were interpreted in terms of a desorption of pyridine from bridging OH groups located in supercages and β-cages,

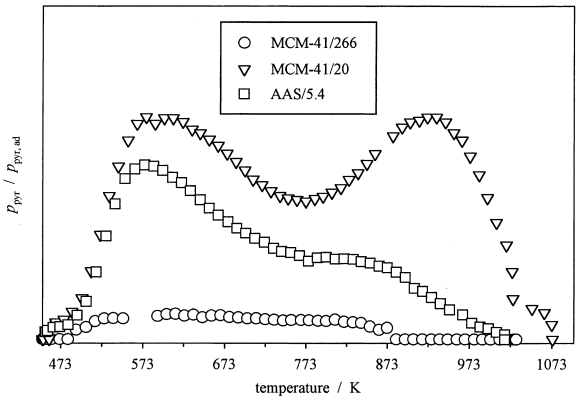


Fig. 3. Temperature-programmed desorption (TPD) of pyridine from the mesoporous materials MCM-41/266 and MCM-41/20 and the amorphous aluminosilicate AAS/5.4.

respectively. TPD experiments of pyridine from dealuminated HY zeolites yielded two additional desorption peaks at temperatures of ca. 600 and 900 K due to weak and strong Lewis acid sites, respectively, formed by extra-framework aluminum atoms [29]. According to these assigments, the pyridine desorption peak observed at 910 K for MCM-41/20 has to be attributed to strong Lewis acid sites. However, a contribution of pyridine molecules strongly bound to Brønsted acid sites to the desorption peaks in the temperature range 700–800 K cannot be excluded.

3.5. FTIR investigations of calcined and pyridine-loaded samples

The FTIR spectra of MCM-41/266, MCM-41/20 and AAS/5.4 recorded in the region of OH stretching vibrations and in the 1400–1700 cm^{-1} frequency region are depicted in Figs. 4 and 5, respectively. The upper spectra were obtained after calcination at 673 K. Adsorption of pyridine molecules at 393 K and subsequent evacuation at 473 K led to the FTIR spectra in Figs. 4 and 5. The region of OH stretching vibrations of the unloaded samples (Fig. 4) consists of a band of terminal silanol groups at 3740 cm^{-1} with a broad shoulder

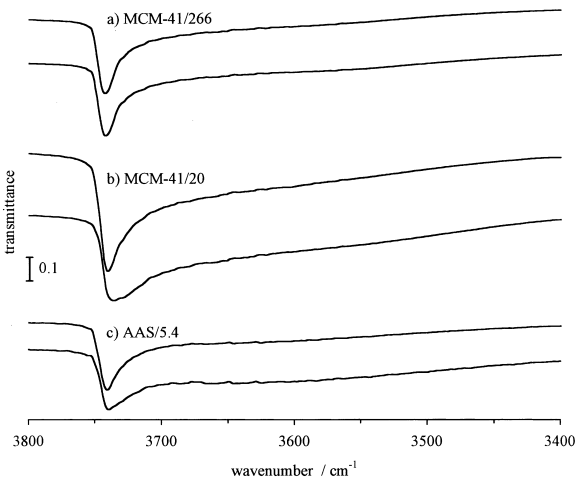


Fig. 4. FTIR spectra of the OH stretching vibrations of the calcined (673 K) mesoporous materials: (a) MCM-41/266; (b) MCM-41/20; and (c) the amorphous aluminosilicate AAS/5.4 recorded before (top) and after adsorption of pyridine at 393 K and subsequent desorption at 473 K (bottom).

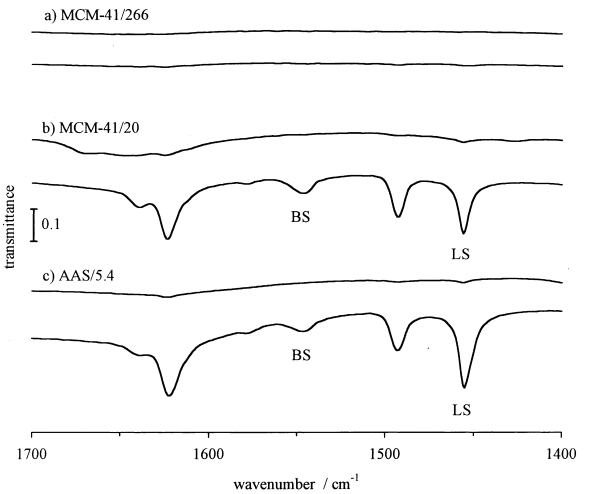


Fig. 5. FTIR spectra of the 1700–1400 cm^{-1} frequency region of the calcined (673 K) mesoporous materials: (a) MCM-41/266; (b) MCM-41/20; and (c) the amorphous aluminosilicate AAS/5.4 recorded before (top) and after adsorption of pyridine at 393 K and subsequent desorption at 473 K (bottom). The bands denoted as BS and LS are due to pyridine molecules interacting with Brønsted and Lewis acid sites, respectively.

at ca. 3710 cm^{-1} due to internal SiOH groups [19]. In contrast to Jentys et al. [19], in the spectrum of the aluminum–containing MCM-41/20 no indication for an additonal band of hydroxyl groups on octahedrally coordinated aluminum atoms (3660 cm^{-1}) was found. This band was found by Jentys et al. [19] in the difference spectrum of the siliceous and aluminum-containing MCM-41 as a broad hump and, therefore, its detection seems to be difficult.

The 1400–1700 cm^{-1} frequency region of the calcined and unloaded samples (Fig. 5, top) consists of weak bands with negligible intensities. Loading of the mesoporous material MCM-41/266 with pyridine (vide supra) does not lead to a significant change in the FTIR spectrum [Fig. 5(a), bottom]. In contrast to this finding, in the spectra of MCM-41/20 and AAS/5.4 loaded with pyridine, strong bands due to C–N vibrations of the probe molecules can be observed in the 1400–1700 cm^{-1} frequency region [Fig. 5(b) and (c), bottom]. According to the literature [19,21,30], the bands at 1545 and 1455 cm^{-1} are due to pyridine molecules strongly bound to Brønsted

(BS) and Lewis acid sites (LS), respectively. The absorption coefficients of these bands amount to $\epsilon_{BS} = 1.670.12$ cm μmol^{-1} and $\epsilon_{LS} = 2.220.21$ cm μmol^{-1} [31], respectively. Hence, a comparison of the number of sites leading to the bands at 1545 cm^{-1} (BS) and 1455 cm^{-1} (LS) requires a multiplication of the integral intensity of the band originating from Lewis acid sites (LS) by a factor of 0.77. Even after this correction of the integral intensities, they indicate that a large number of pyridine molecules remain bound to Lewis acid sites on MCM-41/20 and AAS/5.4 after desorption at 453 K. This finding is in line with the assigment of the high-temperature peaks (at ca. 910 K) in the TPD curves to pyridine molecules previously bound to Lewis acid sites.

Considering the OH stretching vibrations of samples loaded with pyridine, an effect of the probe molecules on the bands of silanol groups can be observed for the aluminosilicates MCM-41/20 [Fig. 4(b), bottom] and AAS/5.4 [Fig. 4(c), bottom]. The FTIR spectra of these samples show bands of pyridine molecules bound at Brønsted acid sites at 1545 cm^{-1} [Fig. 5(b) and (c), bottom] which indicates the presence of silanol groups with an enhanced acid strength. On the other hand, for MCM-41/266 loaded with pyridine neither an effect of the probe molecules on the stretching vibrations of silanol groups [Fig. 4(a), bottom] nor a band at 1545 cm^{-1} [Fig. 5(a), bottom] could be found.

3.6. ^1H MAS NMR spectroscopy of calcined and pyridine-loaded samples

The ^{1}H MAS NMR spectra of calcined MCM-41/266, MCM-41/20 and AAS/5.4 [Fig. 6(a)–(c)] consist of signals in the chemical shift range 1.3–2.2 ppm which are typical for silanol groups in inorganic solids [32,33]. The unsymmetric shape of these signals is a hint for the presence of different types of silanol groups, such as isolated and geminal SiOH groups and internal silanol groups. It is important to note, that the incorporation of aluminum atoms into the framework of MCM-41/20 is not coupled with a broadening of the low-field flank of the silanol signal at 1.3–2.2 ppm, nor does it lead to the appearance

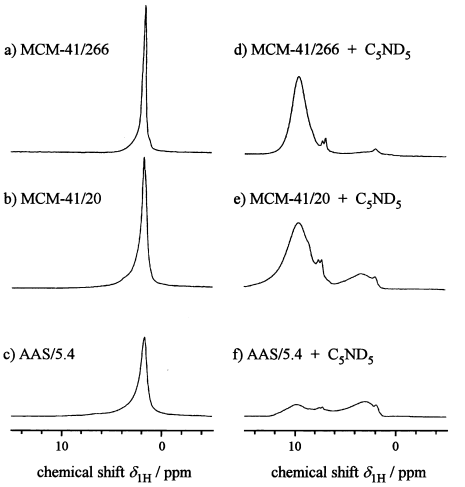


Fig. 6. ^{1}H MAS NMR spectra of the calcined (673 K) mesoporous materials MCM-41/266 [(a) and (d)] and MCM-41/20 [(b) and (e)], and the amorphous aluminosilicate AAS/5.4 [(c) and (f)] recorded before [(a)–(c)] and after [(d)–(f)] adsorption of perdeuterated pyridine.

of additional ^{1}H MAS NMR signals. Using an external intensity standard (zeolite HY-35), the concentrations of silanol groups, c_{OH}, given in column 7 of Table 1 were determined. The comparison of these values with the surface areas, A_{BET}, given in column 3 of Table 1, indicates a correlation between c_{OH} and A_{BET}.

In previous investigations of hydroxyl groups in crystalline and amorphous aluminosilicates, perdeuterated pyridine was applied as a probe molecule allowing a distinction between weak and strong Brønsted acid sites [32]. The adsorption of pyridine on acidic zeolites HY and HZSM-5 leads to a protonation of the probe molecules giving signals of pyridinium ions at 15.5–19.5 ppm. The interaction of pyridine molecules with silanol groups results in the formation of hydrogen-bound adsorbate complexes and shifts the resonance positions of SiOH groups from 1.8 to ca. 9.5 ppm. A similar observation was made after adsorption of perdeuterated pyridine on MCM-41/266, MCM-41/20 and AAS/5.4 [Fig. 6(d)–(f)]. The ^{1}H MAS NMR signals appearing at ca. 9.5 ppm are caused by silanol groups interacting with pyridine molecules via hydrogen bonds. The signals at ca. 2 ppm indicate the presence of non-accessible

internal SiOH groups. The broad lines at 3.5 ppm in the spectra of the aluminosilicates MCM-41/20 and AAS/5.4 loaded with pyridine are due to a small number of AlOH groups [32]. Hydrogen atoms at ring positions of the probe molecules are responsible for the weak signals at 6.8–7.4 ppm.

The low-field signal in the ^{1}H MAS NMR spectrum of MCM-41/20 [Fig. 6(d)] is significantly broader than in the spectrum of MCM-41/266 [Fig. 6(e)]. The left flank of these low-field signals reaches 15 ppm. A contribution of thermal motions to this broadening effect can be excluded, since the above-mentioned low-field signal exhibits an MAS NMR sideband pattern (not shown). Therefore, the line broadening originates from a distribution of chemical shifts of the low-field signal, probably caused by an interaction of pyridine molecules with silanol groups having different chemical properties.

3.7. ^{1}H MAS NMR and ^{27}Al echo NMR studies of the aluminosilicate MCM-41/20 at different dehydration and calcination steps

It was intended to study simultaneously the interaction of hydroxyl groups with water and ammonia molecules and the local structure of framework aluminum atoms in the aluminum-containing sample MCM-41/20. Therefore, ^{1}H MAS NMR and ^{27}Al echo NMR measurements were carried out on this material in the hydrated state [Fig. 7(a)]; after dehydration at 473 K [Fig. 7(b)]; after calcination at 673 K [Fig. 7(c)]; and after ammoniation and evacuation of the calcined sample [Fig. 7(d)]. Because of the strong broadening of the ^{27}Al NMR signals of aluminum atoms in the frameworks of dehydrated aluminosilicates, these nuclei were investigated under static conditions (without MAS) applying a quadrupole-echo sequence [13,34].

In Fig. 7(a) the ^{1}H MAS NMR and ^{27}Al echo NMR spectra of hydrated MCM-41/20 are depicted. The ^{1}H MAS NMR spectrum shown on the left-hand side is dominated by a signal at 4.7 ppm corresponding to the line position of water molecules adsorbed on silicalite (4.9 ppm [35]) and silica gel (4.8 ppm [35]). The low-field shoulder at ca. 7 ppm is due to ammonium ions introduced by the ion exchange of this material with ammonium nitrate [32]. Interestingly, the ^{1}H MAS NMR spectrum of the hydrated MCM-41/20 agrees well with that of hydrated zeolite NH_4Y [36], but has a significantly stronger signal of water molecules at 4.7 ppm. The ^{27}Al echo NMR spectrum [Fig. 7(a), right] consists of a single signal with a center of gravity at ca. 50 ppm which agrees with the line position of tetrahedrally coordinated framework aluminum atoms observed in the ^{27}Al MAS NMR spectrum [Fig. 2(b), right]. The integral intensity of the ^{27}Al echo NMR signal was set to 100 arbitrary units (a.u.). By ^{27}Al MAS NMR measurements of the hydrated MCM-41/20 at resonance frequencies of 104.3 and 130.3 MHz, no field-dependent second-order quadrupolar resonance shift of the signal at 50 ppm was observed. Therefore, the above-mentioned signal intensity is not affected by quadrupolar interactions.

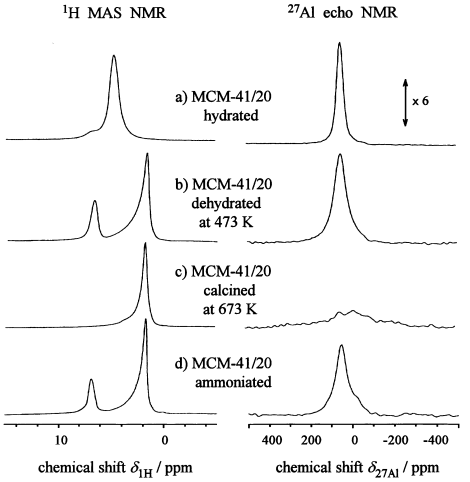


Fig. 7. ^{1}H MAS NMR (left) and ^{27}Al echo NMR (right) spectra of the mesoporous material MCM-41/20 recorded (a) in the hydrated state; (b) after dehydration at 473 K; (c) after calcination at 673 K; and (d) after subsequent ammoniation and evacuation at 473 K.

The spectra shown in Fig. 7(b) were recorded after dehydration of MCM-41/20 at 473 K. The ^{1}H MAS NMR signal of silanol groups at 1.8 ppm corresponds to that in Fig. 6(b). The absence of a signal at 4.7 ppm indicates a complete dehydration of the sample. In the low-field range, only the signal of ammonium ions remains at 6.8 ppm. A quantitative evaluation of this line gives a site

concentration of 0.18 ± 0.02 mmol g^{-1} causing the cation exchange capacity of MCM-41/20 (Table 1, column 8). Furthermore, the dehydration of MCM-41/20 is accompanied by a broadening of the ^{27}Al echo NMR signal of framework aluminum atoms in Fig. 7(b) (right). After Fourier transformation in the absolute intensity mode, the integral intensity of this signal was determined to 28 ± 3 a.u. The only solid-state interaction which is strong enough to cause the intensity distribution between -100 and 200 ppm observed in the ^{27}Al echo NMR spectrum of this sample, is the quadrupole interaction. This assumption is supported by the decrease of the integral intensity from 100–28 a.u. (vide supra). Within the experimental accuracy, the latter value corresponds to the intensity contribution of the central transition ($I_{1/2,-1/2} = 9/35$) of a spin $S = 5/2$ system. A simulation of the ^{27}Al echo NMR signal depicted in Fig. 7(b) (right) using the Bruker software WINFIT yields a quadrupole pattern described by a quadrupole coupling constant of QCC = 5.0 ± 0.2 MHz and an asymmetry parameter of $\eta = 0.6 \pm 0.1$. These values agree with the quadrupole parameters found for tetrahedrally coordinated aluminum atoms incorporated into the frameworks of dehydrated sodium [34] and ammonium forms of zeolites Y and ZSM-5 [37].

The further thermal treatment of MCM-41/20 at a calcination temperature of 673 K leads to a complete deammoniation of the sample. Accordingly, in the ^{1}H MAS NMR spectrum [Fig. 7(c), left] the signal of ammonium ions is absent. Looking at the ^{27}Al echo NMR spectrum [Fig. 7(c), right], the deammoniation is accompanied by a decrease of the signal of framework aluminum atoms (quadrupole pattern with QCC = 5.0 MHz, $\eta = 0.6$) leading to an integral intensity of 4.0 ± 1.0 a.u. Simultaneously, a broad background appears which indicates a variation in the bonding state of the majority of framework aluminum atoms, i.e. in their local geometry and/or oxygen coordination, causing the observed increase in the quadrupolar interaction and line broadening.

The ammoniation of the calcined MCM-41/20 was meant to clarify whether or not the above-mentioned variation in the bonding state of framework aluminum atoms is a reversible process. The calcined MCM-41/20 sample, used to record the spectra shown in Fig. 7(c), was ammoniated at an ammonia pressure of 30 mbar and subsequently evacuated at 473 K for 2 h. A quantitative evaluation of the ^{1}H MAS NMR spectrum depicted in Fig. 7(d) (left) yielded a formation of 0.15 ± 0.02 mmol ammonium ions per gram dry MCM-41/20 responsible for the signal at 6.8 ppm. Hence, the majority (83%) of the sites, which cause the cation exchange capacity of the fresh sample (0.18 ± 0.02 mmol g^{-1}, vide supra), act as Brønsted acid sites after calcination. The strength of these sites is sufficient to protonate ammonia. However, their low concentration in comparison with the whole amount of silanol groups (2.6 mmol g^{-1}) renders their direct observation by FTIR and ^{1}H MAS NMR spectroscopy difficult.

The ^{27}Al echo NMR spectrum of this sample [Fig. 7(d), right] consists of a signal with an integral intensity of 25 ± 3 a.u. and a line shape corresponding to the quadrupole parameters QCC = 5.0 MHz and $\eta = 0.6$ [Fig. 7(d)]. After the reammoniation of the Brønsted acid sites in the calcined MCM-41/20, the majority of framework aluminum atoms show ^{27}Al NMR spectroscopic parameters equal to those of aluminum atoms in the framework of the dehydrated ammonium form aluminosilicate. Hence, the variation of the bonding state of framework aluminum atoms going from the ammonium form to the calcined state of the mesoporous aluminosilicate is a reversible process. In addition, this indicates that a connection exists between the chemical state of the Brønsted acid sites and the bonding state of the framework aluminum atoms in this material.

The dehydration, calcination and reammoniation cycle of the amorphous aluminosilicate AAS/5.4 investigated by ^{1}H MAS NMR and ^{27}Al echo NMR spectroscopy yielded similar results as described for MCM-41/20. After dehydration of AAS/5.4 at 473 K, a ^{1}H MAS NMR signal of ammonium ions was found at 6.8 ppm which corresponds to an amount of ammonium ions of 0.06 mmol g^{-1} (Table 1, column 8) due to a corresponding amount of strong Brønsted acid sites. However, the overlap of ^{27}Al echo NMR signals due to aluminum atoms in different oxygen

coordinations [compare Fig. 2(c), left] renders a quantitative evaluation of these spectra difficult.

4. Conclusions

The aim of the present work was the investigation of catalytically active sites in MCM-41 originating from the incorporation of aluminum atoms into the framework of this mesoporous material. Comparing the properties in the ethylbenzene disproportionation, the aluminum-containing sample MCM-41/20 shows an activity which is fourfold higher than that of the siliceous sample MCM-41/266. However, even MCM-41/20 is much less active than typical acidic zeolites, on account of the weaker Brønsted acidity of the former material. The high methanol conversion (51%) found for the siliceous MCM-41/266 as catalyst is due to the formation of dimethylether which seems to be catalyzed at 723 K by non-acidic silanol groups. The consecutive reaction of dimethylether to hydrocarbons, as observed over the aluminum-containing MCM-41/20, is a hint to the presence of Brønsted acid sites. This assumption was supported by the results of FTIR and ^{1}H MAS NMR spectroscopic investigations of MCM-41/20 loaded with pyridine. The spectra recorded were explained by an interaction of the probe molecules with silanol groups which are enhanced in their acid strength, possibly, by an incorporation of framework aluminum atoms in the local structure of a small amount of these hydroxyl groups. The majority of the framework aluminum atoms in MCM-41/20 (aluminum content of 0.794 mmol g^{-1}) are affected in their bonding state by the deammoniation of Brønsted acid sites (0.18 mmol g^{-1}). According to the amounts of these species, it can be speculated that three to four aluminum atoms contribute to the local structure of one Brønsted acid site. Previous investigations of acidic zeolites have shown that bridging OH groups are preferentially located at Si(nAl) sites with the largest possible number of n [38]. Further studies will have to clarify whether this model is valid for Brønsted acid sites in mesoporous aluminosilicates as well.

Acknowledgements

JW and MH gratefully acknowledge financial support by Deutsche Forschungsgemeinschaft, Max Buchner Forschungsstiftung and Fonds der Chemischen Industrie. We thank U. Pingel, Department of Physics and Geophysics, University of Leipzig, for ^{27}Al MAS NMR measurements on an NMR spectrometer MSL 500. We are particularly grateful to Dr H.G. Karge, Fritz Haber Institute of the Max Planck Society, Berlin, for having provided the infrared cell. Thanks are due to M. Hartmann, University of Stuttgart, for assistance in performing the methanol conversion.

References

[1] C.T. Kresge, M.E. Leonowicz, W.J. Roth, J.C. Vartulli, J.S. Beck, Nature (London) 359 (1992) 710.
[2] F. Di Renzo, H. Cambon, R. Dutartre, Microporous Mater. 10 (1997) 283.
[3] C.-Y. Chen, H.-X. Li, M.E. Davis, Microporous Mater. 2 (1993) 17.
[4] C.-Y. Chen, S.L. Burkett, H.-X. Li, M.E. Davis, Microporous Mater. 2 (1993) 27.
[5] W. Kolodziejski, A. Corma, M.-T. Navarro, J. Perez-Pariente, Solid State Nucl. Magn. Reson. 2 (1993) 253.
[6] J. Rathousky, A. Zukal, O. Franke, G. Schulz-Ekloff, J. Chem. Soc., Faraday Trans. 91 (1995) 937.
[7] P.J. Branton, P.G. Hall, K.S.W. Sing, Adsorption 1 (1995) 77.
[8] T. Boger, R. Roesky, R. Gläser, S. Ernst, G. Eigenberger, J. Weitkamp, Microporous Mater. 8 (1997) 79.
[9] I.V. Kozhevnikov, A. Sinnema, R.J.J. Jansen, K. Pamin, H. van Bekkum, Catal. Lett. 30 (1995) 241.
[10] S. Ernst, R. Gläser, M. Selle, in: H. Chon, S.-K. Ihm, Y.S. Uh (Eds.), Progress in Zeolite and Microporous Materials, Studies in Surface Science and Catalysis, vol. 105B, Elsevier, Amsterdam, 1997, p. 1021.
[11] S.D. Djajanti, R.F. How, in: H. Chon, S.-K. Ihm, Y.S. Uh (Eds.), Progress in Zeolite and Microporous Materials, Studies in Surface Science and Catalysis, vol. 105C, Elsevier, Amsterdam, 1997, p. 2067.
[12] D. Trong On, P.N. Joshi, S. Kaliaguine, J. Phys. Chem. 100 (1996) 6743.
[13] C.-F. Cheng, H. He, W. Zhou, J. Klinowski, J.A.S. Goncalves, L.F. Gladden, J. Phys. Chem. 100 (1996) 390.
[14] D.H. Park, C.-F. Cheng, H. He, J. Klinowski, J. Mater. Chem. 7 (1997) 159.
[15] A. Corma, V. Fornes, M.T. Navarro, J. Perez-Pariente, J. Catal. 148 (1994) 569.

[16] M. Busio, J. Jänchen, J.H.C. van Hooff, Microporous Mater. 5 (1995) 211.
[17] R. Mokaya, W. Jones, Z. Luan, M.D. Alba, J. Klinowski, Catal. Lett. 37 (1996) 113.
[18] A. Liepold, K. Roos, W. Reschetilowski, A.P. Esculcas, J. Rocha, A. Philippou, M.W. Anderson, J. Chem. Soc., Faraday Trans. 92 (1996) 4623.
[19] A. Jentys, N.H. Phan, H. Vinek, J. Chem. Soc., Faraday Trans. 93 (1996) 3287.
[20] R.B. Borade, A. Clearfield, in: M. Occelli, H. Kessler (Eds.), Synthesis of Microporous Materials: Zeolites, Clays, and Nanostructures, Marcel Dekker, New York, 1997, p. 431.
[21] J.-H. Kim, M. Tanabe, M. Niwa, Microporous Mater. 10 (1997) 85.
[22] M. Hunger, T. Horvath, J. Am. Chem. Soc. 118 (1996) 12302.
[23] H.G. Karge, K. Hatada, Y. Zhang, R. Fiedorow, Zeolites 3 (1983) 13.
[24] N.P. Rhodes, R. Rudham, J. Chem. Soc., Faraday Trans. 89 (1993) 2551.
[25] U. Weiß, M. Weihe, M. Hunger, G.H. Karge, J. Weitkamp, in: H. Chon, S.-K. Ihm, Y.S. Uh (Eds.), Progress in Zeolite and Microporous Materials, Studies in Surface Science and Catalysis, vol. 105B, Elsevier, Amsterdam, 1997, p. 973.
[26] C.D. Chang, Catal. Rev. Sci. Eng. 25 (1983) 1.
[27] G.J. Hutchings, P. Johnston, D.F. Lee, A. Warwick, C.D. Williams, M. Wilkinson, J. Catal. 147 (1994) 177.
[28] H.G. Karge, V. Dondur, J. Weitkamp, J. Phys. Chem. 95 (1991) 283.
[29] V. Dondur, H.G. Karge, Surf. Sci. 189–190 (1987) 873.
[30] T. Barzetti, E. Selli, D. Moscotti, L. Forni, J. Chem. Soc., Faraday Trans. 92 (1996) 1401.
[31] C.A. Emeis, J. Catal. 141 (1993) 347.
[32] M. Hunger, Solid State Nucl. Magn. Reson. 6 (1996) 1.
[33] M. Hunger, S. Ernst, S. Steuernagel, J. Weitkamp, Microporous Mater. 6 (1996) 349.
[34] H. Ernst, D. Freude, I. Wolf, Chem. Phys. Lett. 212 (1993) 588.
[35] P.H. Kasai, P.M. Jones, J. Mol. Catal. 27 (1984) 81.
[36] H. Pfeifer, D. Freude, M. Hunger, Zeolites 5 (1985) 274.
[37] M. Hunger, T. Horvath, Ber. Bunsenges. Phys. Chem. 99 (1995) 1316.
[38] M. Hunger, M.W. Anderson, A. Ojo, H. Pfeifer, Microporous Mater. 1 (1993) 17.